Surface Analysis of Carbon Steel and Corrosion-Resistant Alloys Exposed to Acid-$SO_4^=$ Chloride Type Geothermal Fluid

James Nogara[1]* and Sadiq J. Zarrouk[2¥]

[1]EnergyDevelopmentCorporation (EDC) - 38th Floor, One Corporate Centre Building

Julia Vargas corner Meralco Avenue, Ortigas Center, Pasig City, 1605, The Philippines

[2]Department of Engineering Sciences, University of Auckland, Private Bag 92019, Auckland, New Zealand

*nogara.jb@energy.com.ph and ¥s.zarrouk@auckland.ac.nz

Keywords: *corrosion, geothermal fluid, CRA, surface analysis, Acid sulphate, low-pH, ESEM-EDS, XRD*

ABSTRACT

Carbon steel and corrosion resistant alloys (CRA) coupons were exposed to low pH acid-$SO_4^=$chloride corrosive geothermal fluid at high temperature and pressure condition. The objective is to gain better understanding of corrosion damage to standard low carbon steels normally used as casing material for geothermal well construction. Corrosion-resistant alloys were likewise evaluated for performance as these may be used as alternative materials in the future. Corrosion tests were conducted in a geothermal production well that has reported casing damage caused by flowing corrosive fluids. Nine types of metals are used for the tests consisting of carbons steels, stainless steels and nickel-base alloys. The corrosion-resistant alloys were selected based on an extensive review of the results of previous geothermal corrosion tests. These metals were exposed to a two-phase acid-$SO_4^=$ chloride type fluid with pH between 3.54 – 3.72 (measured in the laboratory). The corrosive fluid is at a temperature of 170 °C and at low-flow fluid conditions.

Surface evaluation techniques are used to characterize the corrosion behavior of the metals, including coupled environmental scanning electron microscopy – energy dispersive spectroscopy (ESEM-EDS), X-Ray diffraction (XRD), light microscopy and metallographic sample preparation techniques. Results from the tests show that damage to the API standard carbon steel (> 30 days exposure) is significant in this fluid environment in terms of surface penetration either as pitting or uniform corrosion. Generally, the CRA's were resistant to corrosion attack, but a few of the CRA's experienced localized corrosion in the form of pitting. Mineral scales and corrosion products formed on the surface of all the metals tested with varying thicknesses. The scale consists mainly of crystalline zinc sulphide (sphalerite) and minor iron sulfides which deposited from the acid-$SO_4^=$ chloride fluids. Crevice corrosion is intense in carbon steel sections shielded by insulating spacers ("gasket-corrosion") in the acid-$SO_4^=$ chloride fluid environment. Zinc sulfide scales did not form in the crevices. Corrosion product formed in the creviced areas of the carbon steel coupons consists mainly of iron oxide (magnetite) and iron oxy-hydroxides (goethite).

1.0 INTRODUCTION

The number of cases of geothermal wells producing acid-$SO_4^=$ chloride fluid has been increasing as new fields are being developed. This type of fluid is associated with volcano-hosted geothermal systems typical of the fields in Japan(Abe, 1993; Akaku, et al., 2000; Azakawa and Itoi,2009), Philippines (Maturgo, et al., 1996; Suguiaman, et al., 2004), Indonesia (Keserovic, 2013), Costa Rica (Marini et al., 2003; Gherardi, et al., 2005) and possibly Taiwan (Chen, 1970). A few corrosion tests on this type of geothermal fluids have been conducted so far and the more recent work includes Lichti, et al., (2010); Keserovic, (2014) and Keserovic, et al., (2015).

This paper reports on a corrosion experiment that was undertaken to gather more information on the corrosion behavior of carbon steel in a geothermal well that discharge acid-$SO_4^=$ chloride type of fluid. The subject well for this study is currently being produced with significant power output. Despite its productivity, concerns are being raised as to the safety of the well in the future because of corrosion damage. A plan is underway to reline the wellbore with corrosion resistant alloys to extend its productive life. Finding the most cost effective relining material for this well is of utmost importance as it can address the safety issue and at the same time drive down the cost of the activity. With this objective in mind, commercially available CRA's were also tested in this fluid environment together with carbon steel to document their performance and to screen potential candidate materials.

1.1 Background on geothermal well XM-02

XM-02 was drilled in a producing geothermal field in the Philippines in 2011. The well is deviated with a total borehole length of 2,900 meters. Vertical depth reached 2,648 meters. A standard three-string casing design was adopted for the well with the following diameters: 20" conductor, 13 3/8" Anchor and 9 – 5/8" production casings. The production liner is a 7" diameter perforated pipe. The casings and production liners are all made of K55 material. In terms of rock formation, the well penetrated through fresh hornblende andesite lava down to 60 meters, andesite and dacite tuff breccia from about 60 meters down to 2,100 meters and sedimentary breccia with intrusive beyond 2,100 meters of vertical depth. The depths of intersection with the intrusive were not established as the well has been drilled 'blind' from 2,100 meters down to the bottom of the hole. No drill cuttings were returned to the surface beyond this depth for analysis of lithology or alteration mineralogy. Two rock cores were cut at measured depths of 2,114 meters and 2,455 meters to obtain lithological information at the 'blind-drilled' section of the hole.

The hydrothermal alteration of the formation rocks encountered while drilling the well is predominantly neutral-pH consisting of an assemblage of quartz, smectite, illite-smectite, illite, chlorite, calcite, hematite, pyrite and anhydrite. Acid alterations in the rocks consisting of advance argillic minerals were encountered during drilling at the cased-off sections. Sporadic appearances of

crystalline sulfur were also noted at depths from 700-705 meters and from 945-995 meters. Petrographic analysis of the core taken at 2,455 meters noted the presence of weak to moderate adularia in veins and moderate to abundant sericite and pyrite veins. Based on the paragenesis of these minerals, the pH of the fluids at the depth where the core was taken is estimated to be from 5 – 6.

When the well was flowed and subsequently used for production, the fluids had an enthalpy of about 1600 kJ/kg and a reservoir temperature of 320°C estimated from silica geothermometer (TQuartz). This temperature estimate correlates with the feed point temperature measured in the down-hole surveys. The flowed fluid is moderately saline with Cl concentration of about 6,000 ppm. However, the flowed fluid was highly acidic with pH ranging from 3.54 – 3.75 as measured at ambient laboratory temperature. Geochemical modeling of fluids composition at highest wellbore temperature condition showed that the pH decrease only slightly to 3.47.

1.2 Corrosion in Well XM-02

Utilization of the well for production has been limited because of safety concerns on possible wellbore casing and surface pipeline damage due to corrosion. These concerns prompted the operator of the field to conduct a series of down-hole surveys consisting of casing inspection caliper (CIC) and down-hole viewer (DHV) to assess the damage on the wellbore with continued use of the well for steam production. Ultrasonic thickness gauge (UTG) measurements were also frequently conducted on the wellhead assembly to monitor the thinning rate of the equipment while the well was being produced. The first caliper survey was done before the well was flowed and the second survey was conducted after 6 months of continuous production. In addition to down-hole surveys and UTG measurements, an online corrosion monitoring was also conducted in well XM-02 using electrical resistance (ER) probe.

After seven months of discharge, the thickness of the inner casing of the well based on down-hole caliper surveys has been reduced by 23.4% to 37.6%. Some sections of the wellhead assembly have sustained corrosion rates as high as 17 mm/y from the UTG surveys. However, the corrosion rate estimate from the online ER probe is only 0.12 mm/y. It was likewise noted that the corrosion damage was not uniform throughout the length of the borehole casing and in the wellhead assembly. In the casing, corrosion damage appears to be aggravated at the deeper levels compared to shallower sections of the well. At the wellhead, material loss is more pronounced along bends and downstream of constrictions. From this information, the well operators have decided to plan for future intervention in the well before the wall thickness of the casing becomes critical. The plan is to re-line the inner casing the well using a corrosion resistant alloy (CRA). Other corrosion mitigating measures are also being studied including down-hole corrosion inhibitor injection and fluid pH modification (neutralization using caustic soda). These studies are also on-going and may become alternative options if relining proves uneconomic or impractical.

The aim of this test is to expose a number of candidate corrosion resistant alloys (CRA) to the fluids of well XM-02 to observe and document its corrosion resistance properties. This will help in expanding the possible CRA options for the planned work-over relining of the well. The results from the K55 coupon exposure would also validate the observation and results from previous corrosion tests conducted in the well. Since this geothermal well has been producing continuously for an extended period, the fluid chemistry at the time of this experiment can be considered stable. The corrosion rate results from this test whether similar or different from the previous tests would also be useful in projecting qualitatively the long term corrosion damage on the existing casing material in the well. Another objective of the test is to utilize surface methods to evaluate corrosion damage and determine its usefulness in these types of problem.

2.0 EXPERIMENTAL

This section describes the experimental procedure applied during the corrosion test carried-out on well XM-02. Also discuss the stable chemistry of the fluid, the temperature and pressure condition and flow rate at the corrosion test vessel. A short discussion on the metal/alloy used for the test is also included. Finally, the surface evaluation procedure is explained together with instrumentation and the analytical techniques.

2.1 Well XM-02 Corrosion Test Field Set-Up

The corrosion coupon exposure test on well XM-02 was carried-out from June 4, 2014 until July 5, 2014 (32 days). Prior to the test, the well has been flowing continuously since May 2011. Figure 1 describes the layout of the piping system of well XM-02 and the point in the system where the test was conducted. The tapping point location chosen was about 15 meters away from the wellhead and about 4 meters upstream of the production isolation valve (PIV) of the well branch line (16" two-phase pipeline). This branch line eventually merges with a 42" two phase header where the fluids from well XM-02 together with fluids from other wells in the pad mix and travel towards a central separator station. The corrosion test vessel (Figure2) was laid down at ground level. The test vessel was positioned directly below the 16" two-phase pipeline.

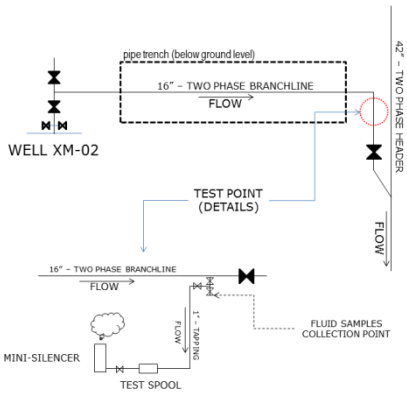

Figure 1. Schematic diagram of the piping layout (not to scale) of well XM-02 showing the position of the test point relative to the well branch line and the 42" two-phase header which led to a central separator.

Geothermal fluid was fed to the vessel through a 1.0” diameter pipe connected to a tapping point in the well branch line. Flow of fluid through the spool was controlled by a throttling valve installed at the downstream piping of the vessel before exiting to a mini-silencer.

The collar of the test coupon rack was pressed in-between two carbon steel orifice plates with 0.1016 m. (4”) diameter orifices. This allowed the rack to be installed in the diametric centre of the spool and held rigidly in place. This also ensured that the coupons nested in the pipe rack were directly exposed to the flow of the geothermal fluid exiting the vessel. Galvanic corrosion on the rack collar or the flanges was prevented by inserting sheets of insulating seals in between the orifice plate, the rack collar and the flange. The test rack was made from Titanium Grade-2 alloy. The flow of fluid passing through the spool was measured volumetrically from the mini-silencer weir using a graduated cylinder and a stopwatch timer.

The pressure and temperature of the fluid inside the test vessel were measured using a pressure gauge and a thermocouple probe meter respectively (Figure 3). The flow of fluid through the spool was monitored regularly with a target flow rate of about 5-10 L/min. The purpose of limiting the flow rate was to ensure that the fluid inside the vessel was constantly replenished but at the same time prevent the effects of high velocity which could initiate erosion effects on the test coupons. The exit valve was adjusted accordingly if the measured flow rate fell out of this range. Pressure and temperature data were also collected and recorded throughout the duration of the test.

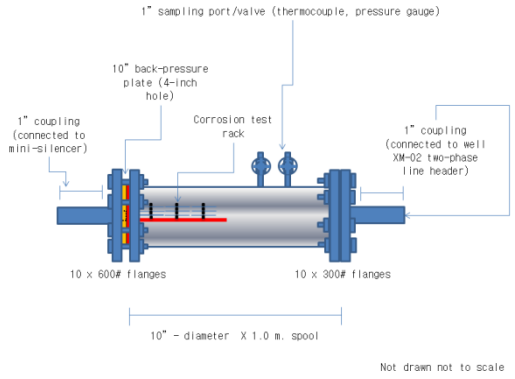

Figure 2. Schematic diagram of the test vessel used in well XM-02 corrosion experiment, two tapping points were mounted on the vessel to accommodate a pressure gauge and a thermocouple probe for measuring pressure and temperature inside the vessel. The test rack was positioned at the diametric center of the vessel parallel to the fluid flow.

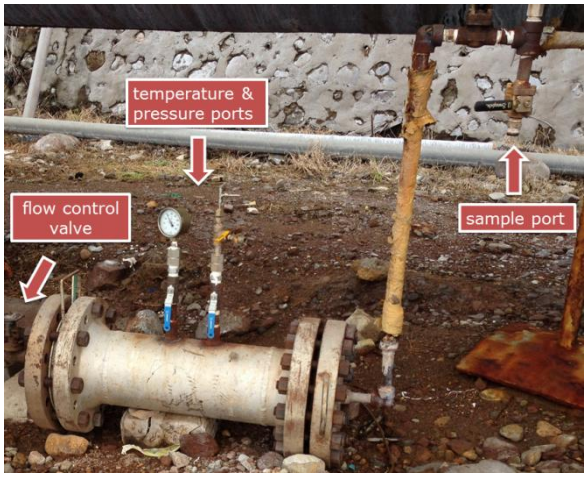

Figure 3. Samples of geothermal fluid were collected from the sample port using a Webre mini-separator. Flow of fluids through the vessel was controlled using the flow control valve during fluid sampling to maintain the flow.

Initially, pressures from the branch line and the test spool were compared when the exit valve of the spool was highly throttled (on bleed). The pressure measured from the well branch line is 0.975 MPa while the pressure inside the test spool was 0.965 MPa (140 psi). There was a slight drop in pressure of 0.01 MPa from the branch line to the spool due mainly to the transition in the pipe diameter. The measured temperature inside the vessel was stable at 179± 2°C. The temperature was close to the saturated steam temperature at the indicated pressure. Pressure, temperature and chemistry of the fluid in the test vessel were essentially identical to the condition inside the branch line.

2.2 Chemistry of Well XM-02 Fluid

The fluid from the well was sampled from the same 1” tapping point that supplies fluid to the corrosion test spool (Figure 3). Care was taken so as not to affect the flow condition in the test spool while fluid samples werebeing collected. The corrosion spool exit valve was throttled when necessary to maintain the pressure inside the vessel at the expense of reduced fluid flow rate. However, this was only temporary as the sampling activity took no more than 30 minutes to complete and the valve were reverted back to original settings afterwards. Sampling for fluid characterization had been conducted weekly. A typical complete chemistry of the fluid is shown in Table 1. Results of chloride and pH trend monitoring during the test together with the flow rate are shown in Figure 4.

Table 1. Chemical composition of fluids from well XM-02 calculated at total discharge (TD) condition except pH. The sample was taken just before the start of the corrosion test. The sampling pressure refers to the pressure in the Webre mini-separator when the liquid and gas samples were collected.

Parameter	Value	Units
Wellhead Pressure	1.05	MPa. abs.
Sampling Pressure	0.991	MPa. abs.
Enthalpy (h)	1,661	kJ/kg
LIQUID		
pH (T)	3.74 (23)	(°C)
Lithium (Li)	10.3	mg/kg
Sodium (Na)	3,074	mg/kg
Potassium (K)	781	mg/kg
Calcium (Ca)	182	mg/kg
Magnesium (Mg)	3.57	mg/kg
Iron (Fe)	25.2	mg/kg
Chloride (Cl)	6,044	mg/kg
Zinc (Zn)*	97.3	µg/kg
Sulfate (SO_4)	147	mg/kg
Bicarbonate (HCO_3)	0	mg/kg
Boron (B)	34.6	mg/kg
Ammonia (NH_3)	12.5	mg/kg
Silica (SiO_2)	1,141	mg/kg
Fluorine (F)	1.78	mg/kg
GAS		
Total Carbon Dioxide (CO_2)	7,309.8	mg/kg
Total Hydrogen Sulfide (H_2S)	830.4	mg/kg
Hydrogen (H)	0.3	mg/kg
Argon (Ar)	0.8	mg/kg
Nitrogen (N)	24.7	mg/kg
Methane (CH_4)	12.5	mg/kg
*data from an adjacent well to XM-02		

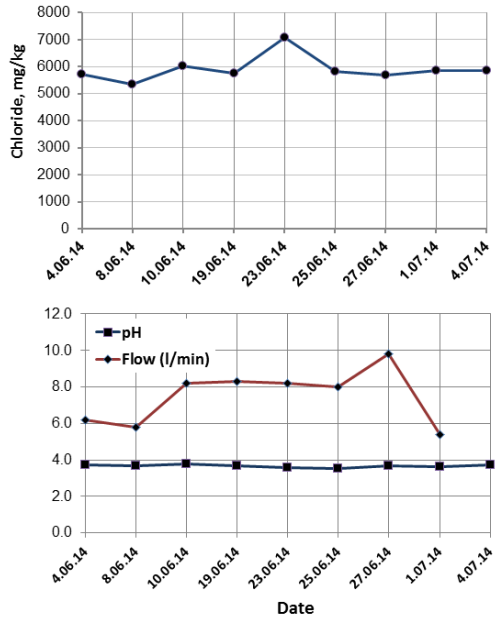

Figure 4. Chloride concentration and pH were stable during the tests showing no significant fluid chemistry changes during the course of the test. Flow of fluid through the test vessel was erratic but did not exceed the allowed flow rate which could cause flow induced erosion-corrosion.

2.3 Corrosion Coupons

Nine types of metal coupons were used for the test. The choice of the corrosion resistant alloys for the test wasbased primarily on the performance of these materials in previous corrosion experiments. Furthermore, cost also plays a role in the selection. All of the CRA's are more expensive than API standard carbon steel used as casing material, assuming same pipe or tubing thickness and dimensions. However, some have costs that are cheaper than the titanium alloys (specifically Beta-C titanium) which are the material of choice for use in the Salton Sea geothermal field (Love, et al., 1988 and Thomas, 2003). If the performance of the cheaper CRA's matches that of the more expensive nickel-base and titanium alloys, then this could significantly drive down the material cost of constructing geothermal wells using CRA's.

The coupons were rectangular shaped with the following dimensions: 3.10 mm (1/8 inch) thick by 19.37 mm (¾ inch) wide by 51.10 mm (2 inch) long and with square corners (tolerances ± 0.79 mm). A 9.55 mm (3/8 – inch) diameter hole was punched at the center of the coupon as suitable bolts insertion to latch the coupon unto the test rack. Alloy codes and sequence numbers were stenciled on the coupon surface near one of the short edges. The coupons were polished using 120-grit (P120 ISO 6344) silicon carbide and weighed to the nearest 0.01 milligram based on ASTM G1 – 90 standard procedures. Details of the materials used for this test can be referenced from Nogara and Zarrouk (2014).

2.4 Corrosion Evaluation

The coupon samples were retrieved after the field corrosion tests. The test rack was un-installed and was allowed to cool to ambient temperature. The coupons were then disengaged from the corrosion rack and rinsed with distilled and de-ionized water to remove non-adherent debris. Afterwards, the coupons were dried in the oven at 60 °C for 30 minutes and stored in desiccators. Prior to transport the coupons were placed in individual sample envelopes and in sealed plastic bags.

2.4.1 Metallographic Techniques

A 1.5 centimeter piece of the metal was cut from edge of each sample coupon. The samples were mounted in clear epoxy mount (two coupons per mount) using hot compression thermosetting technique. The equipment used for hot compression thermosetting was a Struers ProntoPress2^{TM} using the following cycle settings: Force setting of 20 kN, temperature of 180 °C, heat-compression time of 10 minutes and cooling time of 6 minutes. The mount was 3.0 cm in diameter and less than 1.5 cm in thickness.

The mounted samples were then ground using a Struers LavoPol 21^{TM} grinder with the following series of abrasives: P120, P220, P500 and P1200. Once the sample face was exposed and achieved a mirror like sheen, it was then polished using the following series of polishing steps: 6 micron diamond polish in non-woven cloth followed by 3 micron diamond polish on woven cloth and finally, 1 micron diamond polish on napped cloth. No enchants were applied to the sample surface.

2.4.2Environmental Scanning Electron Microscopy (ESEM) and Energy Dispersive X-Ray Spectroscopy (EDS)

Surface scanning of the coupons was performed using an FEI Quanta 200 F™ Environmental Scanning Electron Microscope (ESEM) equipped with a Field Emission Gun. The instrument detector used is Back-scattered Electron Detector (BSE). Quantitative analyses of surface scale and corrosion product on the coupons was carried-out using an EDS with a SiLi (Lithium drifted) detector with a super ultra-thin window.

Two modes of surface scanning were implemented. The first involves high magnification scan of the surface of the metal coupons using backscatter detector and performing an elemental analysis through EDS of the composition of the metal, corrosion products and scales on the surface without pre-processing of the coupons. The second mode involves cutting the coupon in a cross sectional manner to expose the interface between the scale/corrosion product and the substrate metal or alloy. The mounted cross-section samples were coated by platinum conductive coating. Sputter-coating was done using a Quorum Q150R S Modular Coating System to enhance imaging in SEM applications.

2.4.3 X-Ray Diffraction (XRD)

Structural analysis of corrosion products and scales adhering on the surface of the corrosion coupons were done using X-Ray diffraction. This technique provides structural information including interatomic distances and bond angles of the scale and corrosion product crystals. The instrument used was a Bruker D2 PHASER desktop X-Ray diffraction instrument used for analysis of poly-crystalline materials.

2.4.4 Light Microscopy

To identify and document the surface damage caused by exposure of the coupons to corrosive fluid from XM-02, the samples were viewed using a Leica/Wild M420™Photomakroskop (photomicroscope). The coupon samples were placed on a stage directly below the microscope lens and studied for observable defects such as pits, cracks, discolorations and textural differences. The resulting image was stored through an Olympus™ digital imaging system. The resulting image was processed using Photoshop CS6™ to correct for color imbalance and to increase brightness and contrast.

3.0 RESULTS

3.1 Results from Light Microscopy

Figures 6 to 8 shows magnified images of the coupons after 32 days of exposure inside the corrosion test spool in well XM-02. Three images are shown for each coupon as viewed from left to right. The left images show a section of the corner of the coupon, the images in the center shows the appearance of the coupon relative to the portion of the coupon covered by the insulating spacers. The right photo shows the magnified image of a section of the coupon near the stenciled name of the alloy.

It was observed that all of the CRA's were covered with a scale in the section exposed to the fluid consisting of gray to dark brown resinous grains. The thickness of the scale varied across the surfaces of the coupons but generally covered most of the exposed surface. In the section covered by the insulating spacers, the scale was visibly absent and the luster and surface texture of the CRA's in these areas were almost similar to their appearance before exposure to the fluid. Thicker scale deposits were observed to form inside the stencil marks and towards the center of the coupons. When the scale was chipped-off from the surface of the CRA, the appearance of the exposed metal surface was similar to the original color, luster and texture (original grinding scratches).

This resinous scale was also present in both K55 and L80 coupons but only in the exposed areas of the coupons. The color of the K55 coupon (Figure 7, D-F) turned reddish black while the L80 coupon (Figure 6, G-I) turned dark gray to black. The section of the coupons covered by the insulating spacers has also been transformed in color and in texture but different from the exposed surface. Corrosion damage was visible across the surface of both carbon steel coupons. The grinding marks had been eroded to some degree and corrosion craters were visible in K55 (Figure 6, D). Corrosion damage appeared to be more pronounced in the section covered by the insulating washer. Formations of rust tubercles were also evident around the rim of the K55 coupon hole. Numerous microscopic pits were observed in the L80 coupon surface. The corrosion damage in the L80 coupon covered by the insulating spacer was similar to that observed in the K55 coupon. Parts of the stencil marks in the K55 coupon were no longer visible because of corrosion damage in contrast to L80 where the marks were still readable.

The absence of the resinous scale in the shielded areas of both carbon steel coupons was similar to that observed in the CRA's. In contrast, 'rusting' had occurred in the carbon steel coupons whereas; the CRA's appeared to be unchanged. In terms of severity of corrosion damage, the K55 coupon appeared to be more affected than the L80 coupon in the shielded area. The K55 coupon 'rusted' appearance was observed in both shielded and exposed areas, but the damage is more pronounced in the former. There was also a marked difference in the type of corrosion damage incurred by the L80 sample between shielded and exposed surfaces. The corrosion damage in the shielded surface was more uniform corrosion (rusting) while numerous small pits were observed on the exposed surface. Clearly, there was crevice corrosion effect observed for both carbon steel coupons.

It appears that the CRA coupons were immune to this type of corrosion in this fluid environment, with the exception of Alloy-59. There were a few rare pitting sites observed in the creviced surface of the Alloy-59 coupon. It should be pointed out again that underneath the scales that deposited in the exposed surface of the CRA's, the metal were essentially free of corrosion damage.

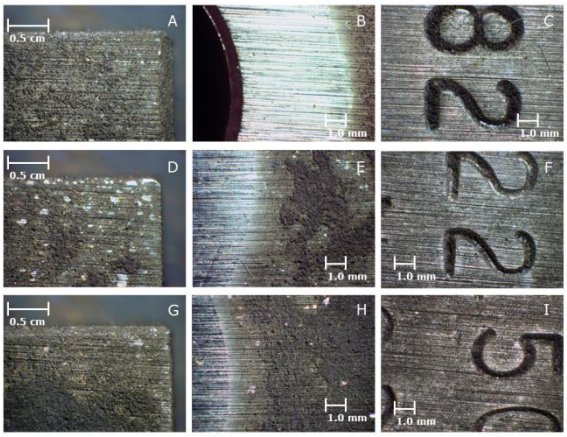

Figure 5. Images of the corrosion coupons after exposure to acid-SO4 chloride geothermal fluid for 32 days viewed from the photomicroscope. A-C: images of Alloy 825 samples taken at the corner of the coupon (A), near the bolt hole which was shielded by insulating spacer (B) and near the stenciled coupon name (C). D-F are images of DSS 2205 while G-I, showed images taken from DSS 2507.

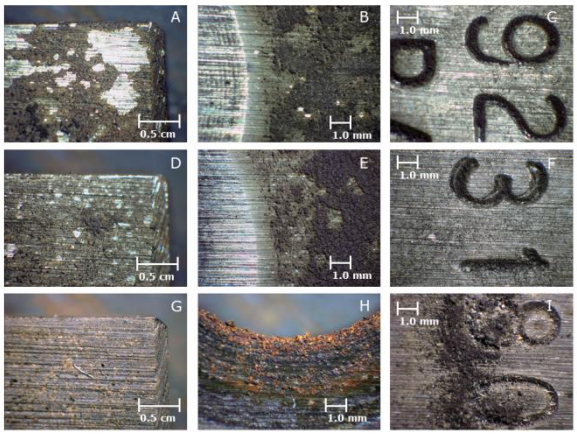

Figure 6. Images of the corrosion coupons after exposure to acid-SO4 chloride geothermal fluid for 32 days viewed from the photomicroscope. A-C: images of Alloy 59 samples taken at the corner of the coupon (A), near the bolt hole which was shielded by insulating spacer (B) and near the stenciled coupon name (C). Photos D-F are images of Alloy31, while G-I showed images taken from carbon steel L80 – Type 1.

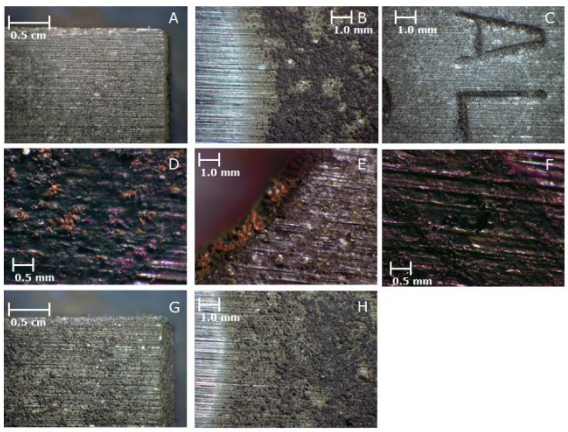

Figure 7. Images of the corrosion coupons after exposure to acid-SO4 chloride geothermal fluid for 32 days viewed from the photomicroscope. A-C: images of AL6XN sample taken at the corner of the coupon (A), near the bolt hole which was shielded by insulating spacer (B) and near the stenciled coupon name (C). Second row (D-F) are images of carbon steel K55 while third row (G-H) showed images taken from Alloy 625.

3.2 Results from Surface Scanning using ESEM-EDS

Figures 9 to 12 show the sample results of surface scanning by ESEM-EDS on the coupons exposed to well XM-02 acid-SO_4 chloride fluids. Each figure shows four scanning electron micrographs taken from the coupons at two areas and magnification level. The two micrographs on the top where taken at low (500×) and high (2000× or 5000×) magnification of the areas in the coupons shielded by the insulating spacer (representing a crevice). At extreme right of the micrographs are the results of the EDS analysis of the shielded area of the coupon. The bottom two micrographs are similar low and high magnification SEM images of the exposed areas of the coupons. To the extreme right, aligned to these images, is the EDS analysis result of the latter. As the visual and light microscopy observations on the coupons reveal clear distinction between shielded and exposed areas, an investigation at high magnification could provide important sub-microscopic information on these differences. This morphologic information together with the elemental composition analyses could shed light on possible metal and fluid interaction in both shielded and exposed coupon surfaces.

The SEM images of the CRA's show clearly that the surfaces of the coupons shielded by the insulating spacers were not covered by scale deposits. The original striation marks caused by grinding with 120-grit abrasives were visible without any deposition or crystalline corrosion product. In contrast, the exposed surfaces of the CRA coupons were partially or completely coated with scale and corrosion product. At high magnifications, the scale consisted of fine crystalline grains that appeared to aggregate to larger crystal structures. The shape of the crystals appeared primarily cubic but with slightly curved faces. There is also clear-cut distinction in the surface elemental analysis results between the shielded and exposed surfaces. As an example, in the AL6XN coupon (Figure 11), the elemental composition EDS scan of the surface essentially mirrored the composition of alloy as specified

by the manufacturer, except for the trace alloy components such as copper, phosphorous and nitrogen which were below the detection limit of the EDS. As far as the major components were concerned, the weight composition was fairly consistent between the EDS result and the composition as provided by the manufacturer. The presence of oxygen and the apparent increase in carbon and silica content in the elemental composition maybe attributed to some specks of impurities or possibly dusts that occasionally settle on the surface of the metal being analyzed.

The result of the EDS analyses scan of the CRA coupons covered with scale deposit was fairly consistent. There was significant percentage of zinc (Zn) and sulfur (S) in the total weight composition, although these elements were not significant (or even trace especially for Zn) component in any of the alloys being tested. The percentage of Zn ranged from 34% – 58% while sulfur ranged from 17% – 25% by weight. In terms of the Zn/S weight ratio, the range is from 2.03 – 3.32. Translated to molar ratio, the range for the CRA's was 0.996 – 1.626. Two alloys yielded a Zn/S molar ratio very close to unity and these were Alloy 59 (0.996) and Alloy 825 (1.006). This means that there were an equal number of atoms of zinc as there was sulfur. It can be postulated at this stage that zinc sulfide (ZnS) could be the likely composition of the scale. In the other cases, sulfur appears deficient with respect to Zn as the ratios were above unity.

With regards to the carbon steel coupons, the appearance of the shielded (creviced) surfaces when viewed at high magnification were very different from the original metal before exposure to the acid fluid from the well (Figures 9 and 10). The grinding marks were considerably eroded and to some extent no longer visible. The surface appeared to show a paste-like mass with 'sandy' texture. 'Cotton-ball'-like globules were also observed forming from the mass. At 5000× magnification (Figure 9, B), some micro-crystals can be observed to grow from this mass of material. The form of these crystals when viewed at high magnification appeared to be isolated hexagonal plates (Figure 13, right image) in the L80 coupon and orthorhombic prisms in K55 coupon (Figure 13, left image). The color contrast between the hexagonal plates and the orthorhombic prisms indicate a difference in molecular mass. Crystal formation habit was also different for both as the hexagonal plates appeared as individual isolated crystals while the prisms form as continuous clusters.

In the exposed surface area of the carbon steel coupons, cubic crystals covered the surface similar to that observed in the CRA coupons. The result of the EDS analysis of the exposed area of the coupons also indicate the presence of large quantities of zinc and sulfur at the same abundance as that detected from the CRA's. Zinc composition by weight ranged from 30.67% – 44.88%, while sulfur was from 18.11 – 19.66%. The Zn/S molar ratio was 0.76 for K55 and 1.35 for the L80 coupon. Contrastingly, in the shielded area of the coupons, zinc was not detected by the EDS, but sulfur was present. Interestingly, the level of oxygen detected (>20% by weight) was unusually high in both coupons in contrast to the CRA's. Formation of iron oxides may explain this abundance of oxygen.

In Figure 12, B microscopic damage was observed on the surface of DSS 2507 at the shielded surface of the coupon. This could be an initiation site for pitting corrosion based on the shape of the damage. The damage appeared to be a circular depression about 25 µm in diameter. Note that this damage was not visible from the optical microscopy inspection.

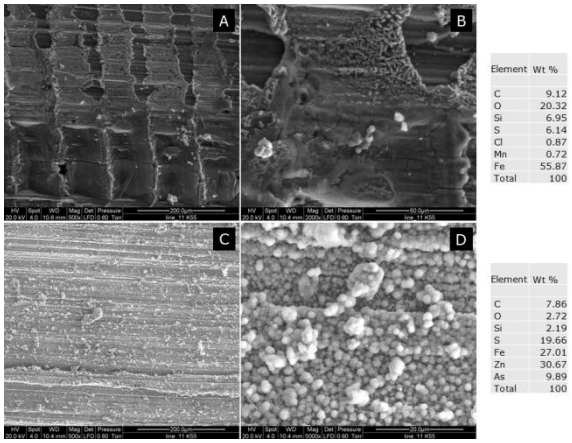

Figure 8. Surface SEM-EDS scan of the surface of K55carbon steel coupon. Top row shows micrographs of the coupon taken from the area shielded (creviced) by the insulating spacer at low magnification (A) and high magnification (B). Bottom rows are micrographs of the area of the coupon exposed to the fluid viewed at low magnification (C) and high magnification (D). Elemental analysis results of the surface scan are shown in tables in the extreme right.

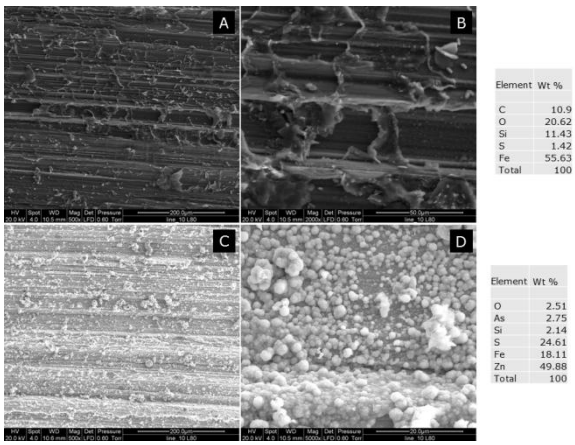

Figure 9. Surface SEM-EDS scan of the surface of L80-Type 1 carbon steel coupon. Top row shows micrographs of the coupon taken from the area shielded (creviced) by the insulating spacer at low magnification (A) and high magnification (B). Bottom rows are micrographs of the area of the coupon exposed to the fluid viewed at low magnification (C) and high magnification (D). Elemental analysis results of the surface scan are shown in tables in the extreme right.

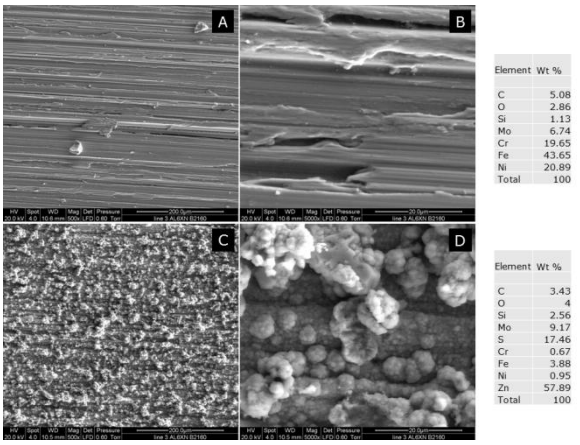

Figure 10. Surface SEM-EDS scan of the surface of AL6XN coupon. Top row shows micrographs of the coupon taken from the area shielded (creviced) by the insulating spacer at low magnification (A) and high magnification (B). Bottom rows are micrographs of the area of the coupon exposed to the fluid viewed at low magnification (C) and high magnification (D). Elemental analysis results of the surface scan are shown in tables in the extreme right.

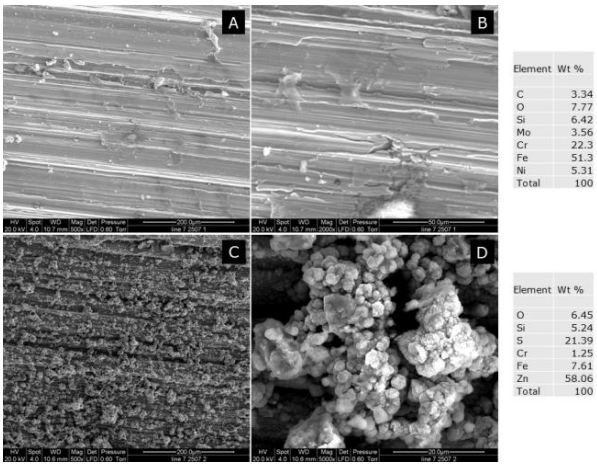

Figure 11. Surface SEM-EDS scan of the surface of DSS 2507 coupon. Top row shows micrographs of the coupon taken from the area shielded (creviced) by the insulating spacer at low magnification (A) and high magnification (B). Bottom rows are micrographs of the area of the coupon exposed to the fluid viewed at low magnification (C) and high magnification (D). Elemental analysis results of the surface scan are shown in tables in the extreme right.

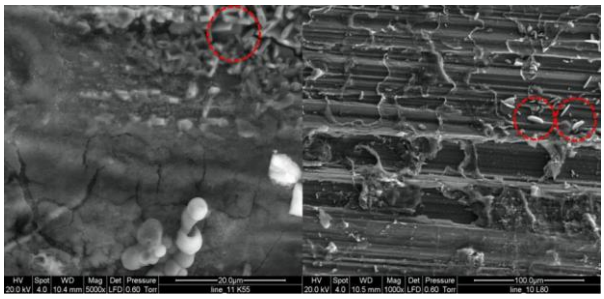

Figure 12. Growth of larger orthorhombic prisms (possibly goethite) from an amorphous mass of iron oxides in the creviced surface of the K55 coupon (Left). Isolated hexagonal plate crystals (possibly troilite) are observed to form in the corroded surface of in the crevice of the L80 – Type 1 coupon (Right).

3.3 Results from X-Ray Diffraction Analysis

Using the DIFFRAC-EVA^{TM} software, the peaks are identified automatically. In some of the coupons, the peak signals from the substrate were also detected from the scaled coupon diffractogram. However, the important peaks are those that do not correspond to the substrate signals as these come from mineral crystals in the scale. Diffractogram pattern matching with existing diffractograms in the software database can be done automatically by providing the likely mineral composition.

In the exposed area of all the coupons tested, zinc and sulfur were ubiquitous and the molecular ratio between the two elements approach unity. With this information, zinc sulfides such as sphalerite and wurtzite diffractograms were tested for possible matches. Very good agreement was obtained for sphalerite (ZnS) in terms of peak intensities at the following interatomic or d-spacing and corresponding 2–θ angles: 3.11 Å (28.66°), 1.91 Å (47.68°), 1.63 Å (56.58°), 1.24 Å (77.05°) and at 2.70 Å (33.21°) (Figure 13). Iron sulfides were also matched and good to fair matches were obtained from pyrrhotite ($Fe_{1+x}S$) and troilite (FeS). Pyrite diffractogram pattern also showed good correlation but a few of the peaks are not identified from sample diffractograms probably because the software was not able to resolve these peaks during automatic peak search. It is also possible that there is very little pyrite in the scale composition which makes the signals very weak. The crystal form of sphalerite is isometric (cubic) hextetrahedral (Shternberg, 1984). This was the prevailing crystal structure observed in the high magnification SEM micrographs of the exposed surface of the coupons.

Based on the EDS analysis results, the XRD from the shielded area of the carbon steel coupons should yield a different set of diffractograms owing to the absence of zinc and the abundance of iron and oxygen. In the scale that formed on the exposed surface, XRD analyses gave poor match with respect to iron oxides including: magnetite ($Fe^{2+}Fe_2^{3+}O_4$), hematite (Fe_2O_3) and maghemite ($Fe_2^{3+}O_3$) and iron oxy-hydroxides: lepidochrocite γ-$Fe^{3+}O(OH)$, goethite (α-$Fe^{3+}O(OH)$)and akaganeite (β-$Fe^{3+}O(OH,Cl)$). Iron carbonate siderite ($FeCO_3$) similarly did not produce good match in terms of diffraction peaks. It is possible that the diffraction patterns of these minerals were masked by

the sulfides owing to their relatively trace amounts within the bulk scale composition.

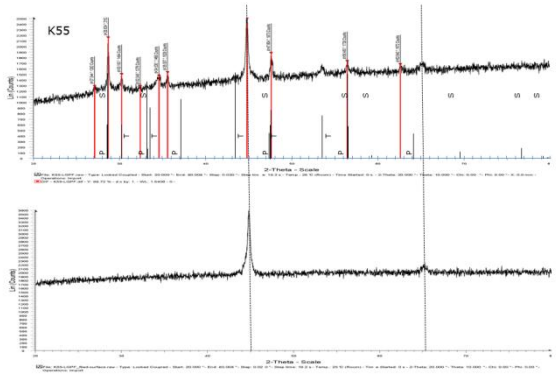

Figure 13. X-Ray diffractograms of carbon steel K55. Pattern of characteristic radiation peaks of the substrate metal (Bottom) and the scaled surface (Top). Also shown in the scaled surface diffractogram are the diffraction pattern of sphalerite (S), troilite (T), and pyrrhotite (P).

3.4 Results from Cross-Section Surface Scan with SEM-EDS

Sample SEM micrograph images of the cross-sections of corrosion coupons are shown in Figures 14 to 17 with magnifications ranging from 2500× up to 16000×. Embedded in the images are the elemental composition analyses from EDS of the scale/corrosion product and the metal. The layers of metal and corrosion products are clearly demarcated by a change in color intensity. This difference is caused by a difference in molecular weight of the compounds in the metal and in the scale.

The purpose of the cross-section scan is to investigate the condition of the metal underneath the corrosion product or scale that covers the surface of the coupon. Other information that may have an impact on corrosion would be the thickness of the scale and if there are changes in scale composition with respect to depth. The cross section scans made in these coupons were in the exposed areas. No scans were made on the shielded section because of the limitation in the dimension of the coupons and again, the position of the bolt holes in the middle of the coupon posed a constraint in mounting the sample.

There was no observable damage or defect to the metal surface underlying the scale such as pitting or cracking in the Alloy-625 coupon (Figure 15). The same is true for Alloy-31, AL6XN and DSS 2205. Some form of pitting was observed on the surface of duplex stainless steel 2507 (Figure 16). This was also observed in both optical microscope and surface SEM scans within the shielded area of the coupon. In Figure 16, a pit is visible on the left side of the image. The pit formed under a scale of sulfides that were about 10 µm thick. Some isolated small pits were likewise observed in Alloy 825 but because of its rarity, this needs to be further verified with future tests. It was expected that DSS 2507 would be less prone to pitting damage compared to DSS 2205 because of the higher PRE number. In this experiment, 2205 appears to be immune while 2507 showed rare occurrence of pitting corrosion and visible metal damage.

In carbon steel samples, deep pits formed (> 10 µm deep) and interestingly, the pits propagated perpendicular to the pit hole underneath the metal surface. This resulted to formation of sulfide scale underneath a layer of metal. As can be observed in the K55 cross-section (Figure 16), there were alternating layers of metal and scale formed near the surface. The shape of the pit can be clearly seen in the L80 coupon cross section (Figure 17). In the image, a pit with a diameter of about 5 µm formed on the surface of the metal. The pit penetrated to a depth of about 10 µm and hereafter propagated laterally underneath a layer of metal. From there it appears that the deep pit that formed is subsequently plugged by sulfide scales. This explains the observed alternating scale – metal layers as viewed from the cross-section.

The thickness of the sulfide scale that formed on the surface of CRA's was on the average less than 10 µm except for DSS 2507 where the scales formed are thicker than 10 µm (Figure 15). Sulfide scales that formed in the carbon steel coupons were much thicker (> 50 µm) and not including the sulfide scales that interlayer with the metal underneath the pits that developed. It is clear from the EDS elemental analyses of scale from the surface that it was composed mainly of zinc and sulfur and to some extent iron and this scale is a mixture of zinc sulfide (sphalerite) and iron sulfides (troilite, pyrrhotite and pyrite) based on XRD analysis. The same composition was also observed on the elemental analyses of the scales in the cross-section. However, the weight percentage composition of each main component was different. Table 2 shows the values of Zn/Fe and Zn/S molecular ratios based on the surface and cross-section EDS scans of the scales on the coupons. In terms of distance with respect to the original surface of the metal/alloy, the scale analyzed in the cross-section was closer to the metal compared to the scale surface. Zinc was not a component (not even trace amount) of any of the metal and alloys tested in this experiment. However, it was substantially present in the scale that formed on all the coupons. The same was true for sulfur, of which only trace amounts are present in some of the metals. Both zinc and sulfur likely came from the geothermal fluid.

It appears from the Zn/Fe molecular ratios of the scale adhering to the carbon steels that Fe component is more abundant relative to Zn from the cross section (inner) than in the surface of the scale (outer). If the iron sulfide scale formed together with zinc sulfide by precipitation from supersaturated geothermal fluid, it was to be expected that the composition (Zn/Fe) would be fairly constant across (from inner to outer part) the scale. The variation observed in the (Zn/Fe) ratio could be indicating an electrochemical reaction effect in conjunction with precipitation as far as iron sulfide scale is concerned. This could also explain the observed material loss in both carbon steel coupons. Metal oxidation is occurring which leads to formation of iron sulfide corrosion product at the same time as precipitation of zinc sulfides. Sulfur is also noted to be more abundant (relative to Zn) in the cross-section than in the surface scan.

Table 2. Molecular ratios of zinc-sulfur-iron in the elemental analysis of the scale from surface and cross-sectional views.

	MOLECULAR RATIOS			
	ZINC - IRON (Zn/Fe)		ZINC - SULFUR (Zn/S)	
	Surface	X-Section	Surface	X-Section
Carbon Steels				
K55	0.97	9.06	0.77	0.87
L80	2.35	4.24	0.99	1.23
Duplex Stainless Steels				
DSS-2205	5.83	7.33	1.14	1.22
DSS-2507	6.52	9.25	1.33	0.87
Super-Austenitic SS				
AL6XN	12.74	3.26	1.63	1.06
Nickel-base Alloys				
I-625	18.24	23.67	1.28	0.97
I-825	4.53	1.86	1.01	1.97
Alloy-59	14.35		1.00	
Alloy-31	35.71	3.77	1.35	1.23

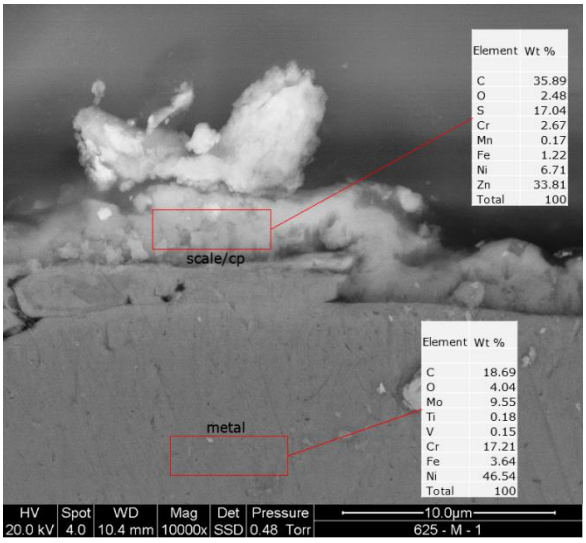

Figure 14. Micrograph of the Alloys 625 with sulfide scale as viewed from the cross-section. The EDS elemental analysis result is shown for both scale and metal to contrast the chemical composition. The scan area is represented by the red rectangle.

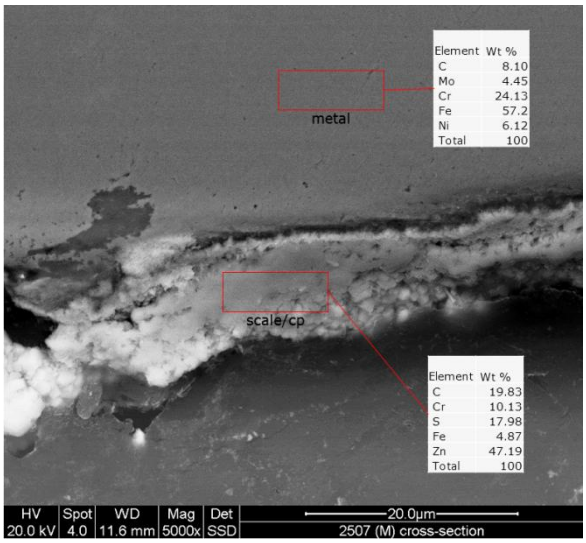

Figure 15. Micrograph of the DSS 2507 with sulfide scale as viewed from the cross-section. The EDS elemental analysis result is shown for both scale and metal to contrast the chemical composition. The scan areas are represented by the red rectangles. A corrosion pit is clearly visible on the left side of the image.

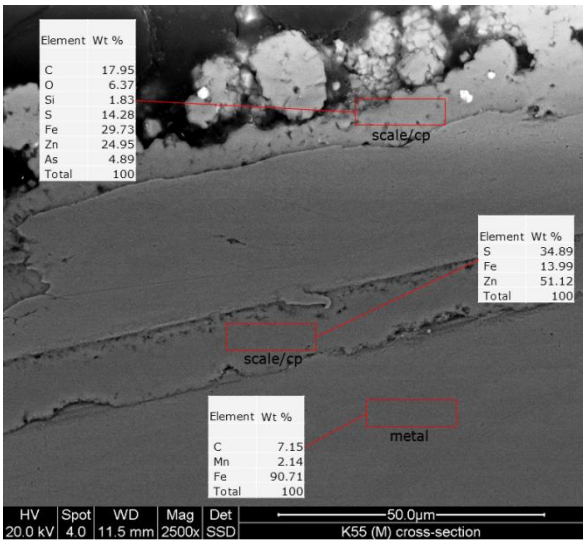

Figure 16. Micrograph of the carbon steel K55 with sulfide scale as viewed from the cross-section. The EDS elemental analysis result is shown for both scale and metal to contrast the chemical composition. The scan areas are represented by the red rectangles. Interlayering of metal and sulfide scale is shown in the image.

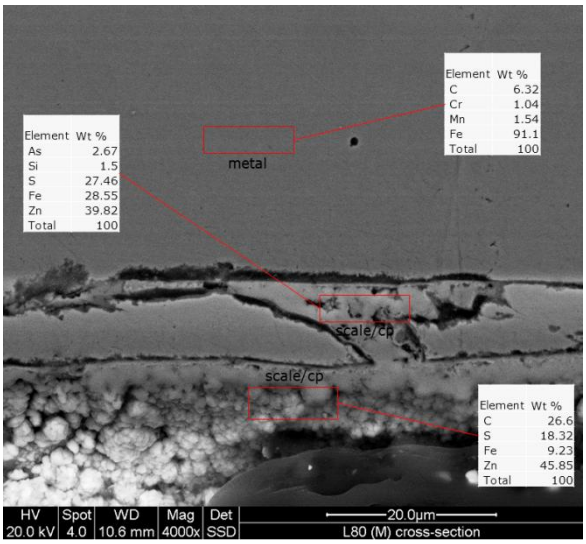

Figure 17. Micrograph of the L80 carbon steel with sulfide scale as viewed from the cross-section. The EDS elemental analysis result is shown for both scale and metal to contrast the chemical composition. The scan areas are represented by the red rectangles.

4.0 DISCUSSION

Table 3summarizes the surface evaluation result of carbon steel and corrosion resistant alloys exposed to acid-SO4 chloride geothermal fluid. Localized corrosion is evaluated in purely qualitative terms and does not attempt to adhere to ASTM G 46 for evaluation of pitting corrosion nor ASTM G 48 for crevice corrosion. Pitting is evaluated based on the cross sections and plan views of the coupons as viewed from the optical photomicroscope and scanning electron microscope. In terms of pitting, qualitative descriptions are used such as abundant, moderate and rare. These observations are not rigorously quantified and serve only to illustrate the presence of pits and the frequency these are observed from the surface scan. This approach is similar to that pursued by Golderg and Owen (1977). The same is true with regards to crevice corrosion. The evaluation method is purely visual and is based on the observed difference between the exposed surface and the surface shielded by the insulating washer. A positive response only means that there is visually clear difference in corrosion attack between shielded and exposed surfaces and that the damage appears to be more pronounced on the shielded surface which indicates crevice corrosion effect. No attempt was made to estimate the corrosion rate based on the thickness of the scale formed. This is mainly due to the analyses result (in the exposed areas of the coupons) which show that the scale consists mainly of zinc sulfide rather than iron oxide or iron sulfide. The percentage of iron sulfide in this scale may be influenced by precipitation from the geothermal solution rather than resulting purely from oxidation of the metal by hydrogen sulfide. Although it is clear from the micrographs that damage to the carbon steel coupons were present and that the metal underwent corrosion. Quantification of the corrosion rate through mass loss method (by ASTM) may be done in future tests. However, care must be exercised in the cleaning procedure as the corrosion observed in the carbon steels shows pits that progress downwards then laterally underneath the sulfide scale that may not be removed by manual brushing with inhibited acid solution. Ultrasonic cleaning may be more effective procedure.

Table 3. Corrosion test result for metal coupons exposed to acid-SO4 chloride type geothermal fluid from well XM-02.

Metal / Alloy	Pitting?	Crevice Corrosion?
K55	Yes (heavy)	Yes
L80	Yes (moderate)	Yes
2205	No	No
2507	Yes (very rare)	No
AL6XN	No	No
625	No	No
825	No	No
3127HMO	No	No
5923HMO	Yes (very rare)	No

The presence of pits, although very rare, in the duplex stainless steel 2507 and in Alloy 59 is surprising especially since DSS 2205 appear to be free of any pits or damage. DSS 2507 has a higher PRE number than 2205 and should withstand pitting corrosion more than the latter. In the case of Alloy 59, which is primarily a nickel alloy (60% nickel) and contains only 1% iron is not expected to experience pitting corrosion. Some studies have indicated the presence of sulfides, specifically manganese sulfide (MnS) as possible initiators of pitting corrosion in stainless steels (Szklarska-Smialowska, 1972; Eklund, 1974; Ryan et al., 2001). This can be considered a possibility although a more detailed experiment specifically for this purpose needs to be conducted to verify the presence of manganese sulfide (MnS) as pit inclusions in both alloys. More comprehensive tests should be done in the future for these materials if these are considered as alternative geothermal well construction materials. Except for these two inconclusive observations, the corrosion resistant alloys show exceptional resistance to corrosion when exposed to acid- SO_4chloride type fluid from well XM-02. The surfaces of these CRA's still retain their shiny metallic luster underneath the iron sulfide scale deposits. The grinding patterns of the original coupon CRA samples are still retained without any visible signs of distortion. For the CRA's, the areas of the coupons shielded by the insulating spacers appear pristine and surface EDS scan of these areas reveal the same composition as the original metal. Scale deposition is negligible or absent altogether.

The carbon steel coupons, the area shielded (creviced) by the insulating spacers incurred substantial damage from uniform corrosion. The scale that developed was mainly iron oxides. Although XRD analyses were not done in the crevice area of the coupons, the Fe/O weight ratio from the elemental analysis is fairly consistent at 2.69 – 2.75 close to the magnetite ratio of 2.62. One possible explanation for the absence of sphalerite-iron sulfide deposits inside the shielded area in all the coupons is that the geothermal fluid is not able to penetrate inside the crevice because of the tightness of the fit of the insulating spacers. This supports the notion that the scale is actually deposited from solution and without the fluid, deposition cannot occur. An alternative explanation is that, the acid geothermal fluid actually penetrated inside the crevice but because of the restricted flow, a micro-environment was created which

was not conducive to sphalerite deposition but rather to electrochemical corrosion which produced magnetite. Previous studies (Potter and Mann, 1965) on steel corrosion show that non-protective multi-laminated magnetite scales form in the surface of steel exposed to acidic aqueous solutions without H_2S at high temperature.

Although the exact mechanism for this unusual crevice corrosion behavior observed in the carbon steels will not be resolved in this study, a definitive answer to this phenomenon will have significant impact as far as expected damage in geothermal wellbores transporting acid geothermal fluids. In crevices created inside the casing joints of the geothermal well, multi-laminated magnetite may form. The formation of non-protective magnetite is of concern because of its rapid growth rate and because it is able to continue growing in filled crevices, producing a volume increase and exerting a considerable 'jacking' force against an external restraint" (Robertson and Forest, 1991). If this occurs in the threaded casing joints, it may cause the joints to crack or fail and eventually lead to parted casings along the joints especially in well with this type of acidic fluids. This can potentially lead to the formation of steam thief zones, loss of well productivity and high risk of well blowout.

Result from the analyses done on the metal coupons that were exposed to the fluid show that the scale is a mixture of zinc and iron-sulfides specifically sphalerite, pyrrhotite and troilite and possibly small amounts of pyrite. Formation of sphalerite scale in carbon steel pipelines transporting geothermal fluids has been documented by a number of authors (Criaud and Foulliac, 1989; Akaku, 1990; Akaku, et al., 1991; Ajima, et al., 1998; Ward, et al., 2006 and Hardardottir, 2011). In most cases, sphalerite scale formation has been associated with acidic geothermal fluids and also exists in conjunction with other minerals such as tetrahedrite – $Cu,Fe)_{12}Sb_4S_{13}$ (Ajima, et al, 1998), galena – PbS (Akaku, et al, 1991), and chalcopyrite – $CuFeS_2$, galena and bornite – Cu_5FeS_4(Hardardottir, 2011). Sphalerite is known to precipitate in natural geothermal systems from hydrothermal fluids as a result of a wide range of processes (Reed and Palandri, 2006; Tagirov and Seward, 2010). The proposed hydrothermal reaction for sphalerite formation is:

$$ZnCl^+(aq) + H_2S(aq) \rightarrow ZnS(sphalerite) + 2H^+(aq) + Cl^-(aq)$$

Metal complexation by aqueous Cl^- and HS^- ligands keeps the zinc ions in solution preventing sulfide mineral precipitation until changes in fluid temperature, pressure or pH favor the deposition process (Akaku, et al., 1991; Reed and Palandri, 2006). The iron sulfides (pyrrhotite, troilite and pyrite) have also been observed to form together with sphalerite in natural hydrothermal deposits by the diffusion of aqueous sulfide into wall rock (Reed, 1997).

Ultimately, the question whether these mixed metal sulfide scale that deposited on the surface of the metal protects it from excessive corrosion damage needs to be answered. The relationship between passive-film formations composed of iron oxides specifically magnetite in high temperature corrosion of steel has been widely studied (Robertson, 1989).The typical boiler water iron oxide protective films that form at high temperature consist of duplex type consisting of an inner layer of fine-grained oxide and an outer layer of loosely packed, larger grains magnetite scale which grow according to a parabolic time law (Potter and Mann, 1965). Such dual layer oxides are not seen in geothermal waters. In acid solutions, a thick multi-laminated film grows according to a linear time law and is not considered protective. In the creviced area of the carbon steel corrosion coupons used in this test, magnetite layers have formed mainly fine-grained but appear to transition to larger crystal grains in some sections. This is not expected to develop into multi-laminated film but could potentially expand and cause damage to crevice areas in the wellbore casing string.

High-temperature corrosion in aqueous solutions containing dissolved H_2S leading to the formation of iron sulfide corrosion products, e.g. mackinawite, troilite, pyrrhotite, pyrite have also been extensively studied. Specific information on the effects of deposited zinc sulfides scale (sphalerite) on the corrosion rate of carbon steel in aqueous solution was not found in the literature search. However, because troilite, pyrrhotite and pyrite exist in the scale deposit, it is fair to assume that the effect to the corrosion behavior would mirror that exhibited by these iron sulfides. Pyrrhotite film growth on the surface of steel is found to reduce corrosion rates or carbon steel with time based on experiments conducted on 'sour gas' environments (Sun, et al., 2011). Sphalerite is a weaker semi-conductor than iron sulfide. Thus, it can be inferred that the deposition of sulfide scale from well XM-02 could retard the uniform corrosion rate of the carbon steel casings. But it should be emphasized that pitting corrosion is still observed underneath the sulfide scale formed but the corrosion rate is probably less than what would be expected from a uniform corrosion without the scale.

It is also possible that the observed high corrosion rate at the bottom casing of well XM-02 than at the surface (as measured from the caliper survey) could be a function of the degree of sulfide scaling inside the wellbore. It is postulated that, sphalerite scaling maybe increasing in thickness from the bottom of the well towards the surface. Because of this, uniform corrosion is the primary mechanism for material loss near the well bottom which produces a high corrosion rate (rapid thinning). Towards the surface, the thick metal sulfide scale prevents uniform corrosion rate by forming a metal – environment barrier where transport of reactive species is dependent on diffusion rates through the sulfide scale. Corrosion persists despite the presence of the sulfide scale adhering to the surface of the metal but the casing may be susceptible to localized corrosion, mainly pitting. This may also explain the relatively low corrosion rate for carbon steel observed in the ER probes (0.12 mm/y) and in the coupons used in this test compared to that observed in the casing inspection caliper.

When this scale is mechanically removed either through the action of the high-velocity fluids especially those that have significant carry-over solid particles, it is expected that uniform corrosion rate would occur. This could explain the high corrosion rates observed along pipe bends such as in the pipe bends and constrictions. The combined effect of this corrosion – erosion is more detrimental to the casings and pipes.

5.0 SUMMARY AND RECOMMENDATIONS

Exposure of carbon steel and corrosion resistant alloys to acid-SO_4 chloride geothermal fluid with a pH of 3.6 in this experiment yielded the following observations and conclusions:

1. The corrosion resistant alloys used in the test, with the possible exception of DSS 2507 and Alloy 59 did not sustain any corrosion damage after 32 days of exposure to acid-$SO_4^{=}$+ chloride type geothermal fluid with a pH of 3.6 at an average temperature of 179 °C. DSS 2507 and Alloy 59 sustained rare instances of pitting, and may require re-validation tests. The pitting is observed mainly on the creviced area of the coupon.

2. The areas of the coupons exposed to the acid geothermal fluid were covered with a thin adherent scale consisting of mainly of sphalerite (ZnS) and minor amounts of iron sulfides: troilite, pyrrhotite and rare pyrite. The thicknesses of the scales vary for each type of metal, but the trend shows increasing thickness from nickel-base/superaustenitic alloys to DSS 2507 to carbon steel.

3. The creviced areas of the coupons underneath the insulating spacers did not form any sphalerite/iron sulfide scale on any of the coupons tested. In the case of the CRA's, the surface of the coupons in the crevices retained their pre-experiment luster and surface texture and appear to be unaffected by corrosion based on microscopic observation and compositional analyses. The carbon steels (K55 and L80) on the other hand showed significant damage in the creviced area in the form of general corrosion and pitting. Surface analysis of the metal showed transformation of steel to iron oxide primarily magnetite.

4. In the exposed areas of the coupons, underneath the cover of sphalerite/iron sulfide film, the CRA's did not sustain any observable material loss or corrosion damage other than the occasional pitting observed on DSS 2507 and Alloy-59. In contrast, deep pits were observed underneath the sulfide scale in both K55 and L80 coupons. The pits (hole-diameter of < 10 µm) penetrate about 10 µm below the surface of the metal and propagate laterally. These pits were observed to be filled-out eventually by sulfide scale.

5. The apparent difference between the corrosion rates measured from the carbon steel ER probe and the calculated based on casing inspection caliper maybe explained by the effect of formation of sulfide scale and the effects of fluid velocity. Pitting becomes the dominant form of corrosion in the presence of the sulfide scale instead of uniform corrosion. When the scales are absent or are removed mechanically through the action of high fluid velocity, uniform corrosion dominates.

With the results and findings of the tests conducted, the following recommendations are forwarded:

1. Except for Alloy 59 and DSS 2507, the rest of the CRA's showed immunity to corrosion (uniform, pitting and crevice) under exposure to acid-$SO_4^{=}$+ chloride geothermal fluid flowed by well XM-02. Future re-lining of the damaged well may consider the use of any of these alloys depending on which is most cost effective. Further tests are recommended for these alloys using constant-strain test (U-bend coupons) to evaluate resistance of these alloys to stress-corrosion. Note that wellbore casing are subject to extreme stress during cycles of shut-in and discharging conditions.

2. In surface pipelines made from carbon steel that are straight and fluid flow is not turbulent, sulfide scales can thicken and protect the metal from high corrosion rates. With time, corrosion rates may drop further from the current 0.12 mm/y. Replacement of these pipes with CRA material may not be necessary. However, pitting corrosion is still expected to occur. To address this problem, doubler plate maybe installed in sections of the pipes that have experienced complete perforation caused by pitting. In carbon steel pipeline sections where fluids are at high velocity and flow is turbulent, erosion-corrosion is expected. Failure is expected in this pipeline sections, replacement of these sections with CRA's may be implemented either as a protective plate or as whole pipe. In the former, the CRA material, carbon steel, and weld material need to be tested for compatibility with regards to galvanic corrosion.

3. The casing joints in the well where crevices form maybe especially vulnerable to crevice corrosion as observed from the results of the tests on carbon steel materials. Sulfide scales do not form inside these crevices. Instead uniform and pitting corrosion occur leading to the formation of (possibly) multi-laminated magnetite. Continued thickening of this corrosion product may exert pressure on the joint threads which can lead to failure. These joints should be regularly inspected for signs of deformation.

4. Other possible solutions to the corrosion need to be studied. Cathodic protection, which is widely used to protect well casing in the oil and gas industry may be considered also in geothermal well applications. However, most of the application in oil and gas is casing corrosion outside of the casing rather than inside. A study on possible cathodic protection designs for inside casing application is recommended.

5. In similar corrosion tests in the future, it is recommended that multiple sets of coupons be used to enable a wider range of analyses to be conducted. Cross-sectional views of the metal coupon surface offer insights into the nature of corrosion occurring beyond the information available from mass loss data but tests should include both mass-loss and metallographic observations. More research is needed in quantifying the effects of scaling or mineral deposition on the rate of corrosion of carbon steel. This is especially true in geothermal fluids where different types of scales form as a result of variations in fluid chemistry.

REFERENCES

Abe, M. (1993).Long term use of acidic reservoir at Onikobe geothermal power plant. Proceedings of the 15th New Zealand Geothermal Workshop, pp. 5-10.

Akaku, K., Reed, M. H., Yagi, M., Kai, K., & Yasuda, Y. (1991).Chemical and physical processes occurring in the Fushime geothermal system, Kyushu, Japan.Geochem. J, 25, 315-333.

Akazawa, N., & Itoi, R. (2009). Analysis of neutralization reaction in a geothermal well.PROCEEDINGS, Thirty-Fourth Workshop on Geothermal Reservoir Engineering

Stanford University, Stanford, California, SGP-TR-187, 9 pages.

Arnórsson, S., Bjarnason, J. Ö.,Giroud, N., Gunnarsson, I., &Stefánsson, A. (2006). Sampling and analysis of geothermal fluids.Geofluids, 6(3), 203-216.

ASTM G 1. (2011) "Standard Practice forpreparing, cleaning and evaluatingcorrosion test specimens". ASTM.West Conshohocken, PA.

ASTM G111 – 97 (2013) "Standard Guide for Corrosion Tests in High Temperature or High Pressure Environment, or Both".ASTM International.

Bäßler, R., Klapper, H. S., Feigl, M., &Hilker, N. (2014, May).Corrosion Resistance of High-alloyed and Alternative Materials in an Artificial Geothermal Water.In CORROSION 2014.Paper No. 3826, 8 pages, NACE International.

Bäßler, R., Keserović, A., Sobetzki, J., Klapper, H. S., &Dimper, M. (2015).Materials Evaluation for Geothermal Applications in Different Geothermal Waters.Materials Evaluation, 19, 25.

Baboian, R. (2005). Corrosion tests and standards: Application and interpretation (2nd edition): (MNL 20) () ASTM International.

Bai, P., Zheng, S., Chen, C.,& Zhao, H. (2014). Investigation of the Iron−Sulfide Phase Transformation in Nanoscale.Cryst. Growth Des., 14, 4295−4302

Baessler, R., Burkert, A., Saadat, A., Kirchheiner, R., & Finke, M. (2009).Evaluation of corrosion resistance of materials for geothermal applications.CORROSION 2009.

Casper, L. A., & Pinchback, T. R. (1980). Geothermal scaling and corrosion : Symposia presented at New Orleans, La., 19-20 Feb. 1979, and Honolulu, Hawaii, 4-5 April 1979 / L.A. Casper and T.R. Pinchback, editors Philadelphia, Pa. 1916 Race St., Philadelphia 19103 : American Society for Testing and Materials c1980.

Castle, J. E., & Mann, G. M. W. (1966).The mechanism of formation of a porous oxide film on steel. Corrosion Science, 6(6), 253-262.

Chen, C. H. (1970). Geology and geothermal power potential of the Tatun volcanic region.Geothermics, 2, Part 2(0), 1134-1143.

Conover, M., Ellis, P., & Curzon, A. (1980).Material selection guidelines for geothermal power systems–An overview. Geothermal Scaling and Corrosion: Symposia Presented at New Orleans, La., 19-20 Feb. 1979, and Honolulu, Hawaii, 4-5 April 1979, (717) pp. 24.

Cornell, R. M., &Schwertmann, U. (2006). The iron oxides: Structure, properties, reactions, occurrences and uses. John Wiley & Sons. New York: New York: VCH 1996.

Einarsson, K., Pálsson, B., Gudmundsson, Á.,Hólmgeirsson, S., Ingason, K., Matthíasson, J., …Armansson, H. (2010). Acid wells in the Krafla geothermal field. Proceedings of the World Geothermal Congress, pp. 1-6.

Fleet, M. E. (1971).The crystal structure of a pyrrhotite (Fe_7S_8).Acta Crystallographica Section B: Structural Crystallography and Crystal Chemistry, 27(10), 1864-1867.

Fournier, R. O., & Potter, R. W. (1982).Revised and expanded silica (quartz) geothermometer. Bull., Geothermal Resource Council (Davis, Calif.);(United States), 11(10).

Goldstein, J. I., et al. (2003) Scanning Electron Microscopy and X-ray Micronalysis, 3rd edition, Plenum Press, New York.

Hardardóttir, V. (2011). Metal-rich scales in the Reykjanes geothermal system, SW Iceland: sulfide minerals in a seawater-dominated hydrothermal environment. PhD Thesis. Department of Earth Sciences – Faculty of Science, University of Ottawa (Canada)

Harrar, J. E., Fischer, J. W., Beiriger, W. J., Steele, W. J., Digiallonardo, S. A., & McCoy, D. D. (1979). Incipient processes in the corrosion of mild steel in 90°C hypersaline geothermal brine. Corrosion Science, 19(7), 819-833.

Hauksson, T., Markusson, S., Einarsson, K., Karlsdóttir, S. N., Einarsson, Á.,Möller, A., …Sigmarsson, P. (2014). Pilot testing of handling the fluids from the IDDP-1 exploratory geothermal well, Krafla, N.E. Iceland.Geothermics, 49(0), 76-82.

Holligan, D., Cron, C., Love, W., & Buster, J. (1989). Performance of beta titanium in a Salton Sea field geothermal production well. SPE/IADC Drilling Conference

Ikeuchi, J., Sanada, N., Asano, O., Kurata, Y., Odawara, O., &Okahara, Y. (1982). Fundamental research on the assessment of materials exposed to geothermal environments. Energy Dev Japan (Chicago), V 5(N 1), 51-79.

Keserović, A., &Bäßler, R. (2013).Material evaluation for application in geothermal systems in Indonesia. Corrosion 2013

Kiyosu, Y., &Kurahashi, M. (1983).Origin of sulfur species in acid sulfate-chloride thermal waters, Northeastern Japan.GeochimicaetCosmochimicaActa, 47(7), 1237-1245.

Kurata, Y., Sanada, N., Nanjo, H., &Ikeuchi, J. (1995). Casing Pipe Materials for Deep Geothermal Wells,

Lichti, K. A. (2007). Forgotten phenomenon of materials selection and use in geothermal energy applications. Materials at High Temperatures, 24(4), 351-363.

Lichti, K. A., Soylemezoglu, S., &Cunliffe, K. D. (1981). Geothermal corrosion and corrosion products.Proceeding of the New Zealand Geothermal Workshop, pp. 103-108.

Lichti, K. A., Swann, S. J., &Sanada, N. (1997).Corrosion in volcanic hot springs (No.CONF-971048--).Geothermal Resources Council, Davis, CA (United States).

Lichti, K. A., White, S. P., Ko, M., Villa Jr, R. R., Siega, F. L., Olivar, M. M. M., ...&Sanada, N. (2010). Acid Well Utilisation Study: Well MG-9D, Philippines. In Proceedings World Geothermal Congress, Bali, Indonesia (pp. 25-29).

Lichti, K., Klumpers, A., &Sanada, N. (2003).Utilisation of acidic geothermal well fluids progress to 2002.Proc 25th NZ Geothermal Workshop, pp. 197-202.

Lichti, K.A., Engelberg, &D.,Young, M.G. (1999). Corrosion in simulated acidic geothermal well fluids. 21st New Zealand Geothermal Workshop, 1(1), 187-192.

Love, W., Cron, C., &Holligan, D. (1988).The use of beta-C titanium for downhole production casing in geothermal wells.Sixth World Conference on Titanium. I, pp. 443-448.

MacDonald, D. D., &Syrett, B. C. (1979).Potential-pH diagrams for iron and nickel in high salinity geothermal brine containing low concentrations of hydrogen sulfide. Corrosion, 35(10), 471-475.

Magaly, F. A., Miguel, R. M., Rigoberto, T. A., & Fernando, S. M. (2010). The neutralization of acid fluids: an alternative of commercial exploitation wells on Los Humeros Geothermal Field. In World Geothermal Congress, Bali, Indonesia.

Manfredi, C., Mozhi, T., & Wilde, B. (1989).Corrosion of carbon steel in saturated brine at 150°C – the effects of pH. Corrosion, 45(2), 172-177.

Marini, L., Yock-Fung, A., & Sanchez, E. (2003). Use of reaction path modeling to identify the processes governing the generation of neutral Na–Cl and acidic Na–Cl–SO4 deep geothermal liquids at Miravalles geothermal system, Costa Rica. Journal of Volcanology and Geothermal Research, 128(4), 363-387.

Maturgo, 0.0., 1996, Chemical characteristics of acid fluids in some PNOC geothermal wells, 17th PNOC-Energy Development Corporation Geothermal Conference, Manila, Philippines, 111-117.

MR0175/ISO 15156 (2003).NACE International, Houston, Texas.

Nogara, J. B., Alincastre, R. S., &Dulce, R. G. (2002). Long term use of production wells with acidic discharge at Mindanao-2 power station, Mindanao geothermal production field (MGPF), Philippines. Twenty-Seventh Workshop on Geothermal Reservoir Engineering,

Nogara, J., & Zarrouk, S. J. (2014, November).Evaluation of Corrosion Resistant Alloys as Construction Material for Acidic Geothermal Wells.In Proceedings 36th New Zealand Geothermal Workshop (Vol. 24, p. 26).

Reed, M. H., & Palandri, J. (2006).Sulfide mineral precipitation from hydrothermal fluids. Reviews in Mineralogy and Geochemistry, 61(1), 609-631.

Robertson, J. (1989). The mechanism of high temperature aqueous corrosion of steel. Corrosion Science, 29(11–12), 1275-1291.

Robertson, J. (1991). The mechanism of high temperature aqueous corrosion of stainless steels. Corrosion Science, 32(4), 443-465.

Salonga, N. (1996). Fluid and mineral equilibria in acid NaCl (SO_4) reservoir: The case of Sandawa Collapse, Mt. Apo hydrothermal system. Proc. 17th Annual PNOC-EDC Geothermal Conference, pp. 119-129.

Sanada, N., Kurata, Y., Nanjo, H., &Ikeuchi, J. (1995).Material damage in high velocity acidic fluids (No.CONF-951037--).Geothermal Resources Council, Davis, CA (United States).

Sanada, N., Kurata, Y., Nanjo, H., Kim, H., Ikeuchi, J., &Lichti, K. A. (2000). IEA deep geothermal resources subtask C: Materials, progress with a database for materials performance in deep and acidic geothermal wells. Proceedings of World Geothermal Congress, International Geothermal Association (IGA), may, pp. 2411-2416.

Shannon, D. W. (1978). Sampling and analysis methods for geothermal fluids and gases.NASA STI/Recon Technical Report N, 79, 27679.

Shoesmith, D. W., Taylor, P., Bailey, M. G., & Owen, D. G. (1980). The formation of ferrous monosulfide polymorphs during the corrosion of iron by aqueous hydrogen sulfide at 21 C. Journal of the Electrochemical Society, 127(5), 1007-1015.

Skála, R., Císařová, I., and Drábek, M. (2006).Inversion twinning in troilite.American Mineralogist, 91(5-6), 917-921.

Smith, J. S., & Miller, J. D. A. (1975). Nature of sulphides and their corrosive effect on ferrous metals: a review. British Corrosion Journal, 10(3), 136-143.

Standard A. S. T. M. G46-94 (2005).“Standard Guide for Examination and Evaluation of Pitting Corrosion,” ASTM International, West Conshohocken, PA.

Standards Association of N. Z. (1991).Code of practice for deep geothermal wells. Wellington N.Z.]: Wellington N.Z.: Standards Association of New Zealand 1991.

Sugiaman, F., Sunio, E., Molling, P., &Stimac, J. (2004).Geochemical response to production of the Tiwi geothermal field, Philippines.Geothermics, 33(1), 57-86.

Takeno, S., Zoka, H. &Niihara, T. (1970).Metastable cubic iron sulfide with special reference to Mackinawite. The American Mineralogist, Vol. 55, September – October, pp. 1639 – 1649

Thomas, R. (2003). Titanium in the geothermal industry.Geothermics, 32(4–6), 679-687.

Truesdell, A., & Nakanishi, S. (2005). Chemistry of neutral and acid production fluids from the Onikobe geothermal field, Miyagi Prefecture, Honshu, Japan.Use of Isotope Techniques to Trace the Origin of Acidic Fluids in Geothermal Systems, 1448, 169.